3 Biotech (2024) 14:230
https://doi.org/10.1007/s13205-024-04072-w

ORIGINAL ARTICLE

The structural insights of L-asparaginase from *Pseudomonas aeruginosa* CSPS4 at elevated temperatures highlight its thermophilic nature

Vinay Kumar[1] · Pragya Anand[2] · Ankita Srivastava[1] · Yusuf Akhter[2] · Digvijay Verma[1]

Received: 29 January 2024 / Accepted: 28 August 2024

Abstract
In the present investigation, a novel thermophilic L-asparaginase (Asn_PA) from *Pseudomonas aeruginosa* CSPS4 was investigated to explore its structural insights at elevated temperatures. Sequence analysis of Asn_PA depicted three conserved motifs (VVILATGGTIAG, DGIVITHGTDTLEETAYFL, and, LRKQGVQIIRSSHVNAGGF), of them, two motifs exhibit catalytically-important residues i.e., T^{45} and T^{125}. A homology modelling-based structure model for Asn_PA was generated with 4PGA as the top-matched template. The predicted structure was validated and energy was minimized. Molecular docking was carried out cantered at the active site for asparagine and glutamine as its substrate ligands. The enzyme–substrate interaction analysis showed binding affinities of −4.8 and −4.1 kcal/mol for asparagine and glutamine respectively. Molecular dynamics (MD) simulation studies showed a better stability of Asn_PA at temperatures of 60 °C, over 40, 50 and, 80 °C, making this enzyme a novel L-asparaginase from other mesophilic *P. aeruginosa* strain. The trajectory analysis showed that RMSD, Rg, and, SASA values correlate well with each other in the different tested temperatures during the MD analysis. Thus, the present findings encourage extensive characterization of the Asn_PA using laboratory experiments to understand the structural behavior of the active site loop in an open or closed state with and without the substrate molecules.

Keywords L-asparaginase · *Pseudomonas aeruginosa*, · Thermophilic enzyme, · Homology modelling · Molecular dynamics simulations

Introduction

In the last decade, L-asparaginase has grabbed significant attention due to its applications in the pharmaceutical (Broom et al. 1961; Batool et al. 2016) and food processing industries (Arjun et al. 2016; Cachumba et al. 2016). The enzyme has emerged as a chemotherapeutic agent for treating acute lymphoblastic leukemia (ALL) (Farag et al. 2015; Juluri et al. 2022). By taking advantage of the inability of ALL cells to synthesize adequate l-asparagine (a non-essential amino acid) due to DNA hypermethylation on the gene promoter (Worton et al. 1991; Ren et al. 2004), asparaginases were developed as an anticancer drug (Knott et al. 2018). L-asparaginase hydrolyses available asparagine for leukemic cells and compels them to starving conditions which results in their depletion (Nagarethinam et al. 2012). The other major application of asparaginase has been reported in the starch-based food industry, where asparaginase degrades acrylamide; a suspected carcinogenic and neurotoxic compound (Tareke et al. 2002; Xu et al. 2016). Acrylamide is generated during the deep frying of starch-based food products, where asparagine reacts with reducing sugars at high temperatures under the Maillard reaction (Mottram et al. 2002). Thus, the employment of asparaginase could be considered a safe and cost-effective way to remove the acrylamide without compromising the quality and taste

Vinay Kumar and Pragya Anand have contributed equally to this work.

✉ Yusuf Akhter
yusuf@daad-alumni.de

✉ Digvijay Verma
digvijay.udsc@gmail.com

[1] Department of Environmental Microbiology, School of Earth and Environmental Sciences, Babasaheb Bhimrao Ambedkar University, Lucknow 226025, India

[2] Department of Biotechnology, School of Life Sciences, Babasaheb Bhimrao Ambedkar University, Lucknow 226025, India

Published online: 11 September 2024

of the food. For the food processing industry, thermostable asparaginase could be a better option to treat starch-based food products before frying which can withstand extreme temperatures, whereas, pharmaceutical industries require glutaminase-free asparaginase. There are several reports on thermostable l-asparaginase and a few of them are deficient in glutaminase activity and thus encourage further research to discover novel candidates for asparaginase (Van et al. 2022). Several bacterial asparaginases have been commercialized under different trade names, where asparaginases of *Escherichia coli* and *Erwinia* sp. share the major market (Merck 2000; Tosta et al. 2023). However, both sources exhibit glutaminase activity that leads to allergy and anaphylaxis in long-term usage (Hijiya et al. 2023; Burke et al. 2017).

In recent years, a handful of l-asparaginases of *Pseudomonas* spp. have also been explored (Qeshmi et al. 2022; Patel et al. 2022; Kumar et al. 2022). However, little is known about the structural insights of L-asparaginases of *Pseudomonas* spp. To date, crystal structures of only two asparaginases are available in the PPatel.DB database which is derived from *Pseudomonas* spp. Computation-based methods provide an extensive analysis of the desired protein by quickly exploring its sequence information (Dadwal et al. 2023). As the asparaginase of the present investigation exhibits thermophilic properties [Temperature °C (Topt.) at 60 °] and applicability in the starch-based food industry in acrylamide degradation (Kumar et al. 2024). Therefore, an attempt was made to understand the structural insights of this enzyme to enrich the limited information and understand the amino acids involved in the thermostability of the enzyme at high temperatures.

Methodology

Retrieval of L-asparaginase encoding gene and sequence analysis

The full-length gene (accession no. OR509736) of the asparaginase encoding enzyme of *P. aeruginosa* CSPS4 was investigated using in silico analysis. The gene was translated into a protein sequence by using the ExPASy translation tool (https://web.expasy.org/translate/).

PROTPARAM analysis of the Asn_PA

In silico analysis of the protein sequences was carried out using the PROTPARAM tool (https://web.expasy.org/protparam/) to determine the physico-chemical parameters. It includes amino acid composition, theoretical molecular weight, isoelectric point (pI), extinction coefficient (EC), instability index (Guruprasad et al. 1990), aliphatic index (Ai) [Ikai 1980], grand average hydrophobicity (GRAVY) (Kyte et al. 1982), number of negative (−R) and, positive (+R) amino acids.

Identification of conserved motifs, domains and, signal peptides

The protein sequence of Asn_PA was further analyzed to determine the catalytically active sites, conserved motifs, and other signature sequences using various online tools such as Pfam http://pfam.xfam.organd, Prosite (https://prosite.expasy.org/index.html). To determine the signal peptides, SignalP 6.0 was used to determine the putative signal peptides in asparaginase. Preliminary structural information of asparaginase was determined by secondary structure analysis using ESpript 2.0 software.

Homology modeling and energy minimization of the Asn_PA structure model

Since the crystal structure of asparagine for *P. aeruginosa* was not found in the Protein Databank (PDB) therefore, the homology-based model was performed. A protein-BLAST search against the PDB was conducted to identify the templates for the target sequence, and the templates were selected based on high query coverage and percentage identity. The model prediction of the asparaginase enzyme was done using the Phyre2 [Kelley et al. 2015]. *i*-Tasser (Zhou et al. 2022). and MODELLER (Webb et al. 2016). The generated models were analyzed and validated using SAVES v6.0 and PROCHECK (https://saves.mbi.ucla.edu/) server for secondary structure features and stereochemistry confirmation of the models obtained from all three methods. Further, the best model was prompted to energy minimization using the GROMACS 2021.4 software package to remove any steric hindrances and clashes in the structure. Since the study focuses on understanding the mechanism of the enzyme under different physiological conditions. Therefore, the catalytic behavior of the enzyme was largely analyzed based on the residues in the active site. Consequently, a template-based ScanProSite tool was employed to locate the binding pocket residues, which played a crucial role in understanding the dynamics of the protein under varied conditions. The models were visualized using the PyMoL program (Yuan et al. 2017).

Molecular docking with asparagine and glutamine

The energy-minimized structure of the Asn_PA was further used for molecular docking studies. The receptor and the ligand files were prepared by adding polar hydrogen atoms and by adding the Gasteiger and the Kollman charge using AutoDockTools 1.5.7. The grid map was set around the active

site residues and molecular docking was performed using *AutoDockVina* with asparagine and glutamine as ligands/substrates. A precalculated grid map was set around the active site in the macromolecule. The binding site was calculated based on the amino acid residues present in the pocket. Therefore, the grid box was centralized at amino acid residues present in the active site. The x, y, and, z coordinates of the box were set to (30 × 40 × 30) Å, and the centers were established at 68.86, 85.667, and, 78.279 for the receptor respectively. The docking resulted in nine conformers of ligands in each case, ranked according to their binding energies. The results were reproduced using the same parameters. The best complexes generated were visualized in Discovery Studio 2021 and the two-dimensional plots were studied using LigPlot + (Laskowski et al. 2011).

System setup for molecular dynamic simulations

To understand the effect of temperature on the asparaginase enzyme, a model-based molecular dynamics (MD) simulation studies were conducted using the GROMACS 2021.4 software package (Lindahl et al. 2001). Firstly, the modeled protein structure was energy minimized by applying GROMOS 53a6 force field (Pol-Fachin et al. 2012), and further studies were carried out using the energy-minimized structure (Oostenbrink et al. 2004). The protein was placed in a cubic box and solvated with SPC water molecules with the closest distance of 1.0 nm between the box and the protein. The system was charge neutralized by adding one chloride ion into the system. The prepared system was prompted to energy minimization using the steepest descents method, where the maximum steps were set at 50,000 and the maximum force was less than 10.0 kJ/mol. Before the MD simulation, the four systems were prepared and thermally equilibrated at four distinct temperatures by applying a heat bath, ensuring the desired temperatures for the systems. In this study, the system was scaled to four different temperatures (40, 50, 60, and, 80 °C) to understand the impact of temperature on the dynamics of the Asn_PA enzyme, its active sites, and, the domains (Marti et al. 2021). To achieve the specific temperature of the system, the solvent temperature was adjusted precisely, and the pressure was set at 1 bar, using both NVT (constant number of particles and volume except for temperature) and NPT (constant number of particles, Pressure, and Temperature) ensembles. Eventually, the four production runs for 30 ns were performed for each system. Later, the trajectory analysis and visualization were carried out for the final obtained structure.

Results

Physiochemical analysis of Asn_PA protein based on amino acid residue composition

The full-length gene of l-asparaginase encoding enzyme of *P. aeruginosa* CSPS4 was 1089 bp long and its translated protein exhibits 382 amino acids (Kumar et al. 2024). To predict the physical and chemical analysis of Asn_PA protein, PROTPARAM analysis was carried out. In silico analysis of Asn_PA predicted the molecular mass and theoretical pI of the L-asparaginase enzyme as 38.64 and 7.07 respectively. Amino acid composition analysis identified eight amino acids that showed a relative abundance of more than 5%. It includes alanine (13.5%), valine (9.4%), leucine (8.6%), glycine (7.5%), serine (6.1%), lysine (6.4%), threonine (5.8%), and, asparagine (5.0%). The composition of other amino acids was less than 5%, whereas sulfur-containing amino acids were of methionine (2.8%) type only. Overall, the share of positively (arginine and lysine) and negatively charged (asparagine and glutamine) amino acids was equal in L-asparaginase of this investigation. The estimated half-life of the enzyme was > 10 h in *E. coli* (in vivo). The instability and aliphatic index of the enzyme were 29.80 and 95.72 respectively. The protein showed a grand average hydropathy (GRAVY) index of − 0.02.

Conserved motifs within the active site revealed catalytic residues

The Interpro analysis revealed multiple attributes of the protein sequence. The protein belongs to the l-asparaginase-glutaminase superfamily having three signature sequences at 37–48 (VVILATGGTIAG), 117–135 (DGIVITHGTDTLEETAYFL), 295–313 (LRKQGVQIIRSSHVNAGGF) [Fig. S1**A**]. These regions exhibit two catalytically important amino acids in the regions 37–48 and 117–1235. The Prosite was consistent by showing two catalytic active sites in the first two signature sequences of Interpro outputs. The first catalytically active site was threonine at the 45th position in the putative signature sequence ([LIVM]-x-{L}-T-G(2)-**T**-[IV]-[AGS]), whereas the other one was also threonine positioned at 125th place in the conserved sequence of ([GA]-x-[LIVM]-x(2)-H-G-**T**-D-T-[LIVM]) (Fig. S1B).

Modelled 3D structure shows no local stereo-steric clashes with acceptable geometry

The three-dimensional (3D) structure of the target protein was generated using the Phyre2, *i*-Tasser, AlphaFold, and, MODELLER software. The template used in the

MODELLER was 4PGA as it showed maximum sequence (96%) and structural (88.44%) similarities with the query sequence. Ramachandran's plot assessment showed the maximum number of residues (94.0%) in the favoured region for the models generated using MODELLER, whereas, the structure generated using AlphaFold showed only 86.8% residues in the favoured region (Supplementary Table 1; Fig. S2). Out of the five models generated using MODELLER the third model was found to be the best than the other modelled structures. Based on residues in the favoured regions, residues in the disallowed region, and the DOPE score (−38,579.18), the third model was identified as the best model. The selected model was energy minimized and converged within 1388 steps with a potential energy of −7.1232565e + 06 kJ/mol, using the steepest descent algorithm to remove the steric hindrances and conflicts between the bond lengths and angles. The energy-minimized structure of the protein with the identified active site residues (Fig. 1A). The tertiary structure of the Asn_PA generally comprises α-helices, extended strands, and random coils, which make this protein extensively dynamic. The coordination and conformational role of coils and turns play a crucial role in selectively accepting the preferred substrates. The loop close to the N-terminal acts as a flexible hinge that remains open in the absence of substrate and closes in the presence of substrates (Sigrist et al. 2002; Lubkowski et al. 2020).

Asparagine exhibited better interaction compared to glutamine at the active site

For the molecular docking study, the active site identification was done using the identified ligand-bound homologs and ProSite scan. The identified residues between 39–47 and 118–127 including T^{42}, G^{43}, G^{44}, T^{45}, H^{123}, G^{124}, T^{125}, D^{126}, and, T^{127} residues form the conserved pocket for the Asn_PA enzyme (Fig. 1A). The pocket recites towards the N-terminal domain forming an active site flexible loop with residues T^{45}-P^{65} (Nguyen et al. 2017; Lubkowski et al. 2020). The modelled protein was docked to asparagine and glutamine using AutoDockTools 1.5.7 to generate their various binding modes. The interactions were evaluated through the PyMOL. The asparaginase enzyme had a binding affinity of **−4.8 kcal/mol** with asparagine, where, Thr^{125} and Asp^{126} actively participate in interaction. The amino acids Asn^{201} (bond length = 2.82 Å), Asn^{201} (bond length = 2.83 Å), Thr^{125} (bond length = 2.81 Å), Tyr^{59} (bond length = 3.01 Å) and, Lys^{198} (bond length = 3.12 Å) involved

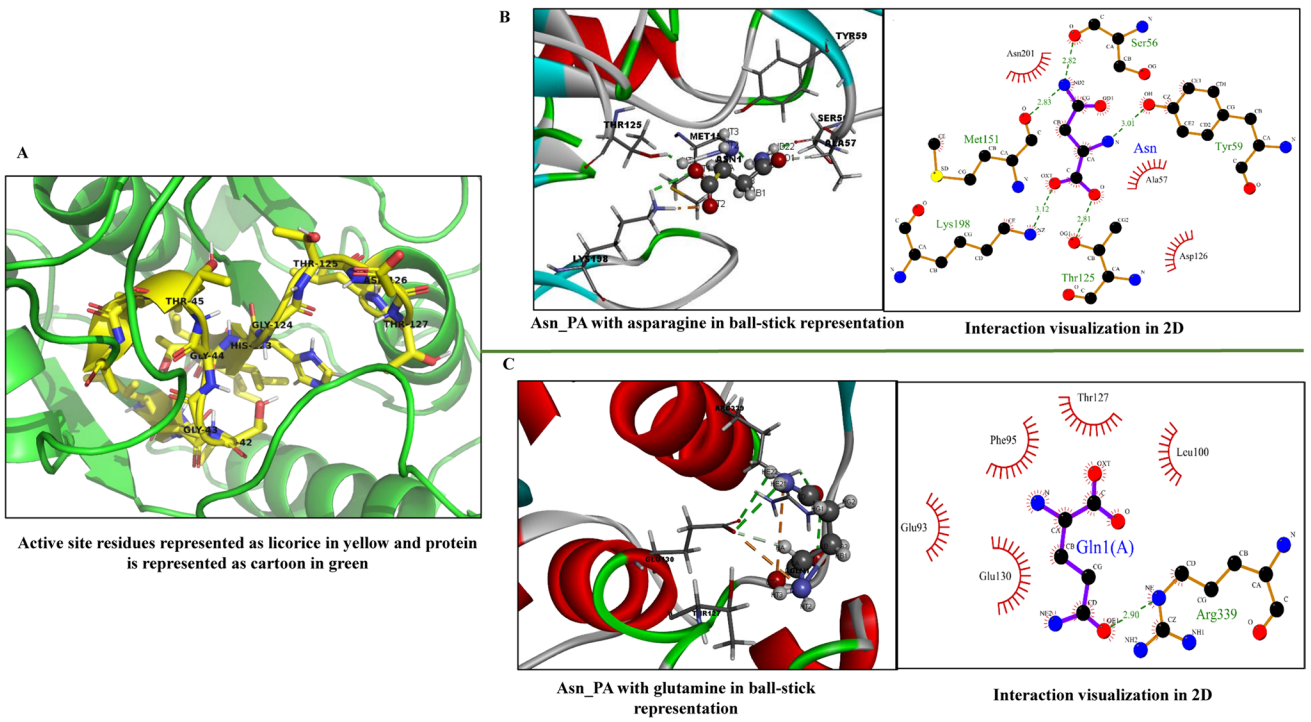

Fig. 1 The Asn_PA protein visualized in green cartoon view with conserved active site residues in licorice format in yellow (**A**). The three-dimensional interaction analysis of asparaginase-asparagine complex showed the residues involved in hydrogen bonding and hydrophobic interactions, along with a two-dimensional interaction plot generated using LigPlot^{+}(**B**). The three-dimensional interaction analysis between the asparaginase-glutamine complex, where ligand is shown in ball-stick representation in grey and the two- dimensional plot for same is generated in right using LigPlot^{+} (**C**)

in hydrogen bond formation, and, Asn^{201}, Ala^{57}, and, Asp^{126} were engaged in hydrophobic interactions with asparagine (Fig. 1B). Whereas, the Asn_PA interaction with glutamine had a binding affinity of **−4.1 kcal/mol**. Interactions involved between glutamine and receptor were with Arg^{339} (bond length = 2.90 Å) forming a hydrogen bond, while Glu^{93}, Phe^{95}, Thr^{127}, Leu^{100}, and, Glu^{130} were involved in hydrophobic interactions (Fig. 1C). The docking results were quite significant as the Asn_PA enzyme showed a higher affinity towards asparagine in comparison to glutamine as substrate. Although, both asparagine and glutamine each have an affinity towards threonine, however, the hydroxyl group of the threonine favourably interacted more with asparagine due to the complementary nature of the functional groups. Thus, the Asn_PA may be interacted favourably with asparagine. The interaction analysis of the receptor-ligand complexes might play an indispensable role in studying the effect of the substrates on the dynamics of the protein.

Elevated temperature induces catalytically more productive conformation

Molecular dynamics simulation was performed to obtain insights into the structural dynamics and conformational changes occurring in the Asn_PA at varying temperatures (40, 50, 60, 80 °C) (Fig. 2). Postost-MD analysis was carried out using RMSD (Root Mean Square Deviation), RMSF (Root Mean Square Fluctuation), Radius of gyration (Rg) and SASA (Solvent Accessible Surface Area) plotting and assessments to evaluate and compare our experimental results with computational results, which are separately evaluated and summarised. Through, the MD analysis, the *Pseudomonas*-specific asparaginase enzyme resembled the experimentally proven data i.e., it was catalytically functional at 60 °C. The flexible gating element (FE) and the hinge region (HR) were responsible for interaction with the substrates such as asparagine and glutamine (Nguyen et al. 2017). It was found that the unmodelled region of the structure, post-simulation transformed into β-sheets at the lowest and maximum used temperatures, whereas, it remained as a coiled loop at 50 and 60 °C temperature. The effect of temperatures was also assessed through the RMSD plots, where the protein from the initial coordinate deviated several folds at 80℃ but obtained a stable conformation before 10 ns. In contrast, at 60 °C the protein after 10 ns showed the most stable conformation and remained less deviated from the initial coordinates indicating more active conformation. The detailed trajectory analysis and relatable results were obtained which are discussed below.

Comparative RMSD at different temperatures reveals that at elevated temperatures the Asn_PA exhibits enhanced thermal stability

The trajectory analysis was performed to obtain deviations in the protein backbone in the different heat baths. We generated RMSD values for the proteins at four different

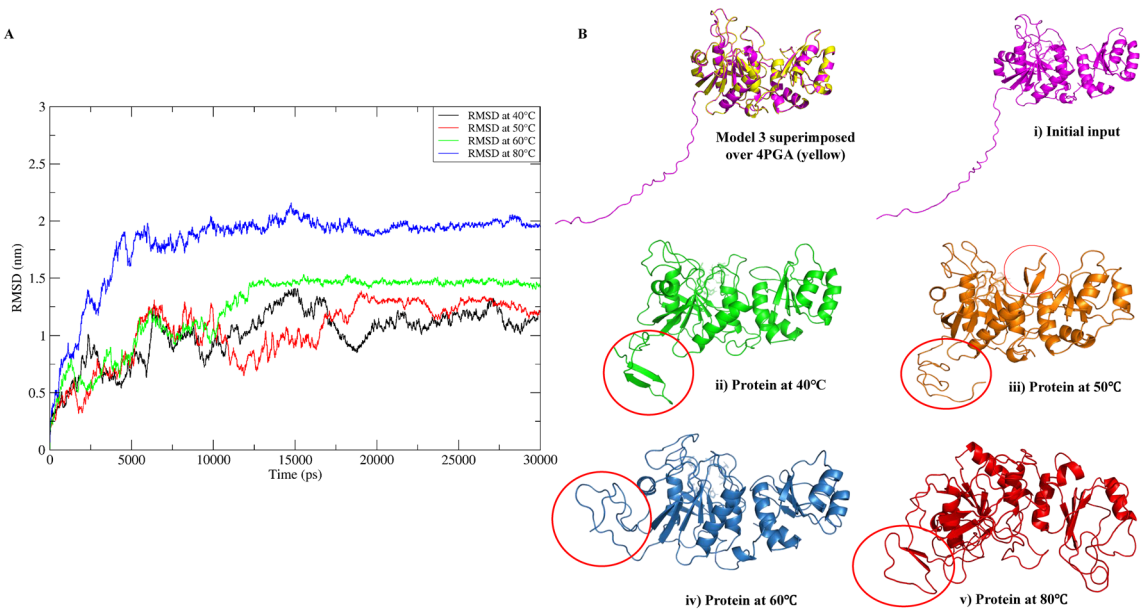

Fig. 2 The Root Mean Square Deviation (RMSD) graph for the three systems (**A**). The green graph shows that the protein at temperature 60 °C, was most stable after the 10 ns run as compared to the protein (Asn_PA) at temperature 40 (black), 50 (red) and 80 °C (blue). The structure visualization for initial input (**i.** magenta), and the protein at 40 (**ii.** green), 50 (**iii.** orange), 60 (**iv.** blue) and 80 °C (**v.** red), which also showed the dynamic structural conversions occurring due to varied temperatures (**B**) encircled in red

temperatures (Fig. 2A). In the graph, the black, red, green, and, blue lines indicate the RMSD values of the protein backbone at 40, 50, 60, and, 80 °C ensembles. While, analyzing the RMSD of individual proteins, the modelled protein at 40 °C showed initial deviations of approximately 1.2–0.000011 nm (negligible) by the end of the simulation. However, through the course of the simulation, the protein exhibited consistent deviations, likely due to the significant transition observed within the N-terminal, specifically snapping residues 6–17. The residues between 6 and17 switched from the unstructured region to the beta-sheet immediately and later formed anti-parallel beta sheets within a time frame of 7 ns as visualized and analyzed (Ji et al. 2019). Anti-parallel beta sheets are the most stable secondary structure folding, which is probably due to the impact of residue composition (a proline at the 9th position) and the temperature e of the surrounding solvent (Shamsir et al. 2007). Furthermore, upon completion of the simulation, the RMSD values demonstrated minimal deviations, suggesting that further simulation calculations could potentially reveal minor structural variations. In the case of protein at 50 °C ensemble, the red graph line reveals continuous deviations. However, in comparison to 40 °C the secondary structure transition occurred in the loop region between residues 196–209, while the unstructured region between residues 1 to 36 remained unstructured at 50 °C but formed a coiled coil-like structure. After approximately 19 ns the structure at 50 °C converged, which in the case of 40 °C, did not occur as notable from the RMSD graph. Furthermore, at 50℃, more pronounced deviations were observed between 10 and 15 ns, indicating frequent conformational change. Also, at 50 °C the RMSD values after 20 ns, deviations reduced to an average of 1.3 nm and by the end of 30 ns negligible deviation was observed as indicated by the RMSD values. At 60 °C, the protein initially deviated for up to 10 ns and thereafter the structure converged. The RMSD values for the enzyme at 60 °C showed initial instability, but comparatively lesser than 40 and 50 °C, which subsequently converged after 10 ns and remained stable. Lastly, at 80 °C a drastic deviation from initial coordinates was observed for up to 6 ns after which the structure is converged. The unstructured region of the protein obtained anti-parallel β-sheet conformation by the end of the simulation. The effect of the temperature of the system on the overall protein structure and dynamics was observed through the comparative analysis of the initial structure (magenta) with the protein structures at 40 °C (green), 50 °C (orange), and 60 °C (blue) and 80 °C (red) [Fig. 2B]. At each temperature, the unmodeled region (1–36 residues) in the N-terminal of the protein exhibited significant transformations, with loops converting into either anti-parallel β-sheets or a coiled-coil structure. These red circles in [Fig. 2B] indicate the highlighted changes. On the other hand, concerning temperatures, the protein remains stable at higher temperatures due to strong thermal packaging, which tends to reduce overall rigidity (Desantis et al. 2022). On the other hand, at low temperatures, the protein adopts a compact conformation, as observed through structural analysis (Liao et al. 2019). The target protein is thermostable and orients a catalytically active conformation at 60 (blue) and 80 °C (red). While, at a temperature below 60 °C, the protein obtains a compact or rigid orientation and shows low molecular motion, due to which secondary structure conversions occur from unstructured loops to β-sheets between residues 6–17 and 196–209. The structural transition was observed immediately when the ensembles were equilibrated at 40 and 50 °C. Over time, these structures further stabilize into well-defined anti-parallel β-sheets. On the other hand, no such secondary structure transition was observed in the protein structure at temperature 60 °C, while at 80 °C the region adopted anti-parallel β-sheets conformation by the end of simulation as well, indicating thermal stability with raised temperature for the protein. In conclusion, the overall structural analysis with respect to RMSD favored the stability of Asn_PA at elevated temperatures. The protein is comparatively more stable and acquires catalytically more favorable conformation at higher temperatures than at lower temperatures. Through, the above analysis we can also hypothesize that the N-terminal region (1–36 residues) of Asn_PA, which did not show similarity with other asparaginases determined structures favors temperature change, which is a signal peptide as identified through InterProScan.

The RMSF analysis revealed favorable relative flexibility of active site flexible regions in the enzymes at elevated temperatures

The asparaginase enzyme comprises of two-domains shown in Fig. 3A, N-terminal (domain 1) and C-terminal (domain 2) domains, consisting of 14 β-strands and 15 α-helices. Each of the domains acquires an α-β-3-layer sandwich conformation for the initial modelled structure as was for *Pseudomonas 7A,* except for the elongated unstructured region between 1 and36 residues for Asn_PA. The domain 1 comprises necessary catalysis elements, including the active site, nucleophilic threonine residue, loop necessary for flexible gating element (FGE), and the hinge region (HR) (Loch et al. 2021). The RMSF were calculated concerning each residue along the length of the protein as shown in Fig. 3B. The HR allocated adjacent to active site loop between G^{43}GTIAGAG^{50} for Asn_PA is identical to *Pseudomonas* 7A and in *P. putida* KT2440 HR at G^{18}GTIAGAG^{25}positions (Jakob et al. 1997; Strzelczyk et al. 2020). The active site flexible loop (ASFL) comprises for residues A^{51}SAANSATY**T**AAK**VP**^{65} where **T**^{60}, $V^{64}$and P^{65} are variant residues for Asn_PA, whereas the residues for respective positions in *Pseudomonas putida*

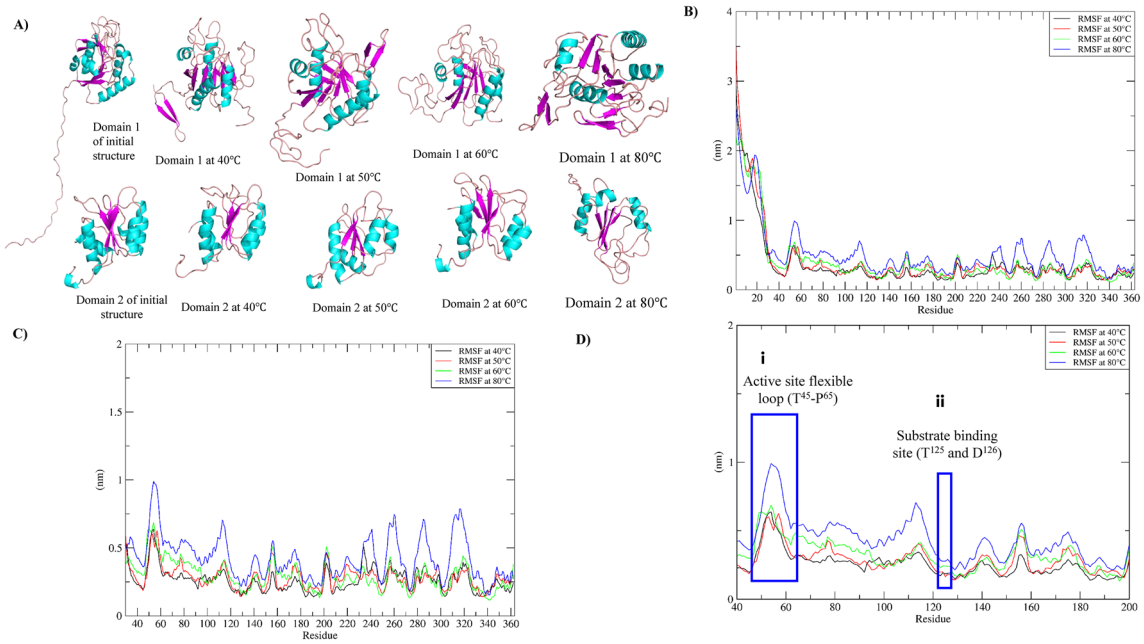

Fig. 3 The secondary structure representation of each domain (N-terminal and C-terminal domains) for initial structure and respective temperature used. Helices (cyan), beta-sheets (magenta), and, loops (light pink) showed the effect of temperatures on the protein structure dynamics (**A**). The RMSF plot of Cα showed higher fluctuation at different temperatures, high flexibility is observed for the unstructured region, residues 1–36 in each case (**B**). The RMSF of protein chain excluding the N-terminal depicted higher fluctuation rate for protein at maximum elevated temperature (blue), the peaks depict the loop region, which becomes prominent at high temperature (**C**). The zoomed-out region between 40 and 200 residues comprising catalytic domain with ASFL (i) and substrate binding (ii) regions highlighted in blue boxes. The RMSF shows subtle flexibility at 60 °C (green), which was low for lower temperatures used (**D**)

KT2440 are Q^{35}, L^{39} and G^{40} and for are *Pseudomonas* 7A Q^{35}, V^{39} and G^{40}. T^{60} is exclusive in Asn_PA species and rest all the residues are conserved. Catalytic sites between residues 39–47 (T^{42}, G^{43}, G^{44}, T^{45}) and 118–128 (H^{123}, G^{124}, T^{125}, D^{126}, T^{127}) as visualized in Fig. 4, the red encircled area depicts the conserved active site residues of asparaginase enzyme identified through PrositeScan (Sigrist et al. 2002; Jakob et al. 1997). The zoomed section of the active site in Fig. 4A, B, C, D, and, E depicts the opened and closed conformation of the loop which is also indicated through the rate of fluctuations in the respective active site residues (Fig. 3B). The side chain visualization of the active site residues clearly shows distortion of active site at 50 °C, whereas initial structure is in a closed conformation, which is followed at 40 °C ensembles, while at 60 °C, the active site appears in an open state. Agreeing with the previous result, the surface area of the catalytic domains for each temperature was such that, 698.42, 740.29, 646.49, 751.90, and 753.96 Å for reference and structures at 40, 50, 60, and 80 °C respectively, which shows that with increasing temperature the accessibility area of catalytic region expands acceptability for diverse substrates. Whilst, at 50 °C, the surface area calculation for Asn_PA appears contradictory, possibly due to the protein's instability as observed in simulation studies. Furthermore, through the calculated RMSF values of each of the systems, the unstructured region in the initial structure showed high fluctuations for each post-MD structures (Fig. 3B). The N-terminal residues from 1 to 36 converted into β-sheet at temperature 40 °C which showed gradual downfall in RMSF values (Fig. 3A), and the peak was between 1.6 to 3 nm. The RMSF value for the N-terminal region at temperature 50 °C reached up to 5 nm, where no secondary structure conversion occurred, indicating low stability and high flexibility in comparison to 40 °C. On the other hand, the RMSF values for N-terminal at 60 °C were between 1 to 1.5 nm indicating the overall structure is dynamically more favorable at this temperature, and the extended N-terminal supports the structure's folding and unfolding at varying temperatures (Bhardwaj et al. 2010). Fundamentally, at high-temperature residues prefer a disordered transition, while acquiring a stronger protein tertiary conformation (Kamalesh et al. 2020), which is also observed from RMSF values of the Asn_PA at 60℃.Where polar residues opt an open orientation facing solvent while the hydrophobic residues tend to be buried. The overall RMSF graph shows minor peaks between 0.5 to 1 nm indicating fluctuations in the loop regions of the Asn_PA in each case (Fig. 3C) by excluding the N-terminal. Furthermore, ASFL between residues T^{45}-P^{65} for the Asn_PA

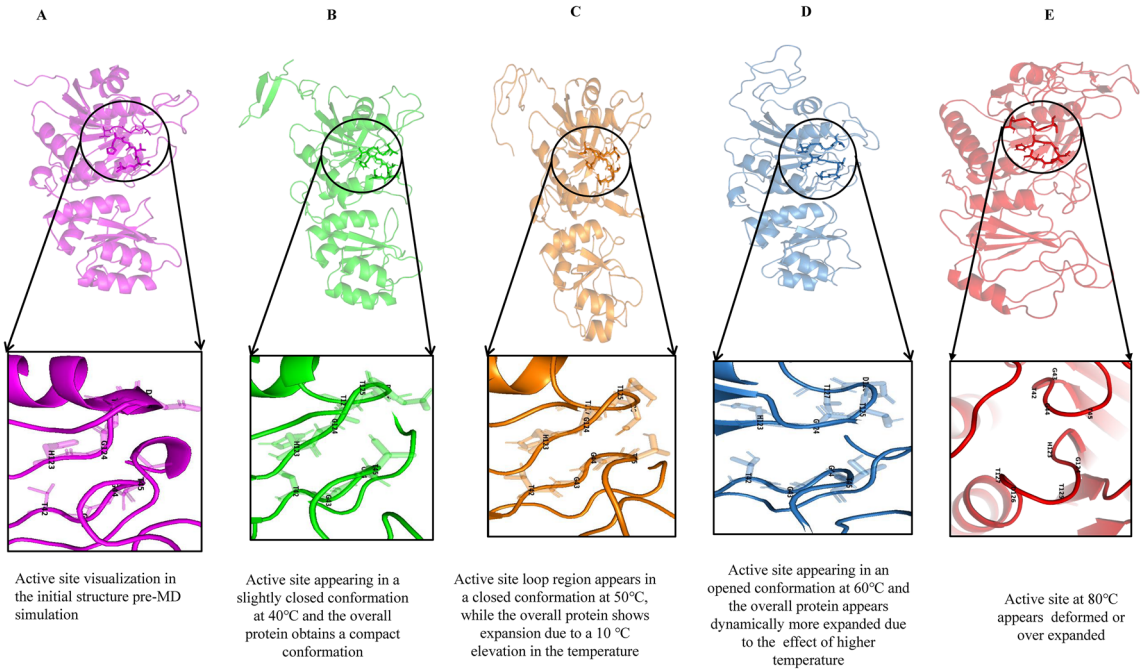

Fig. 4 Active site visualization in the initial structure pre-MD simulation (magenta) (**A**). The active site appeared in a slightly closed conformation at 40 °C and the overall protein obtained a compact conformation due to a low temperature over the other systems (**B**).The active site loop region appeared in a closed conformation at 50 °C which was not a suitable conformation in the absence of any substrate, while the overall protein dynamically appears shredded due to 10 K elevation in the temperature (**C**). The active site appeared in an open conformation at 60 °C and the overall protein showed dynamically more expanded due to the effect of high temperature and open conformation indicating the inactive site (**D**). The active site appeared deformed or expanded at 80 °C (**E**)

enzyme shows subtle fluctuation at 60 °C marked within blue rectangles (Fig. 3D), indicating open conformation and availability of active site residues. The residues at positions $T^{42}GGT^{45}$ and $H^{123}GTDT^{127}$ participated in the binding site formation of the Asn_PA enzyme. The RMSF analysis of these residues suggested that the fluctuation peak is considerably higher at 60℃ as compared to 40 and 50 °C as shown in the blue box (Fig. 3Di). Likewise, for the residues H^{123}, G^{124}, T^{125}, D^{126}, and, T^{127}, the fluctuation at 60 °C (Fig. 3Bii) so feasible flexibility than the other three conditions. This localized subtle flexibility for specific regions suggests a favorable dynamic change, where residues reorient into a catalytically more favorable and functionally enhanced confirmation. Although, on average, the fluctuations for the protein at 60 °C are equivalent to the other two systems, which indicates structure remains intake at this temperature also, while at 80 °C a constrained state of residues is observed for the whole protein. The fluctuations in the catalytic sites are reasonable at 60 °C in comparison to the other systems. In Fig. 4B, C, D, and E the active site regions (39–47 and 118–128) shown as sticks, are responsible for an open or closed conformation as the FGE (Kamalesh et al. 2022). Similar conformational changes were observed post-MD analysis. At 60 °C the loop orients in an open conformation in comparison to the other two systems (Fig. 5). The open state indicates a catalytically active conformation in the absence of substrate (Loch et al. 2021). We hypothesize a close compact conformation for the Asn_PA enzyme in the presence of a native substrate at 60 °C (Kamalesh et al. 2022), which will probably form a firm orientation for ASFL region shown in Fig. 5A. Overall, from the RMSF graph, it is evident that the loop regions exhibit continuous fluctuations, with maximum fluctuation observed in the ASFL (T^{45}-P^{65}) after the N-terminals region (1–36). The structural transitions at the N-terminal occurred due to the altered heat bath ensembles immediately, and did not encourage overall protein stability with respect to temperatures. Besides residues at 60 °C reorient into a stronger tertiary conformation by affecting the flexibility of the loop regions, contributed by thermal stability (Liao et al. 2019; Kamalesh et al. 2020). A similar observation was made at 80 °C, due to the raised temperature the intra and inter-molecular interactions supported the tight protein packing, resulting in a higher fluctuation rate per residue due to adaptability at adverse conditions. The RMSF values at the catalytic site also remain high as shown through the blue line indicating protein at a high strain level due to temperature factor. Eventually, the distance between T^{45}-P^{125} also increased up to 8.4 Å, indicating a wider catalytic site and, thus,

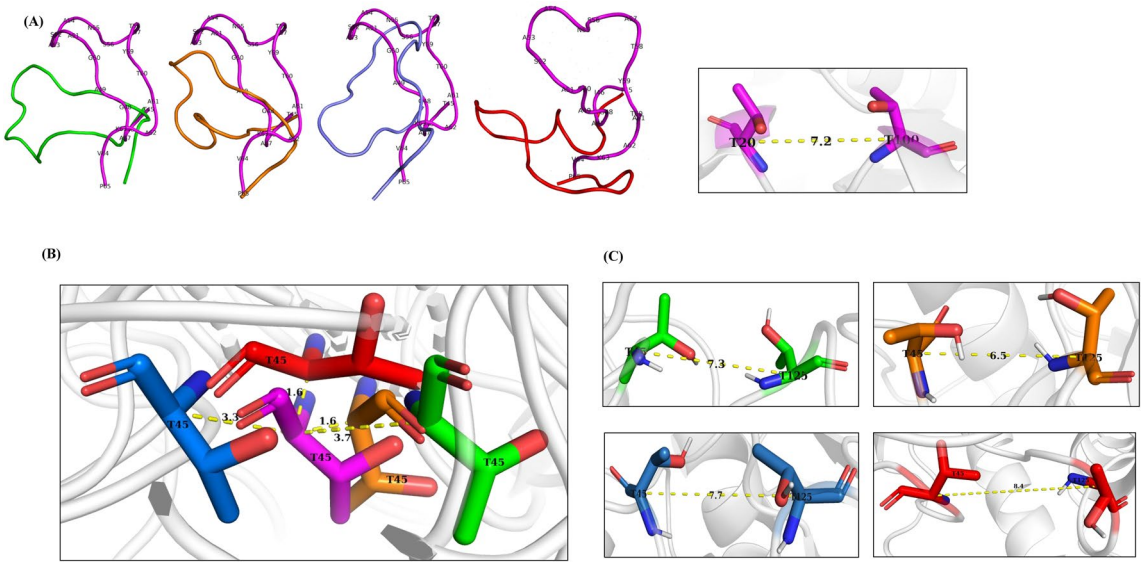

Fig. 5 The flexible active site loop region comprising residues between T^{45}-P^{65}. Following the above color scheme (**A**) showing the deviations occurring with respect to the initial structure loop (magenta) in close conformation, then the loops at 40 (green), 50 (orange) and 60 (blue) and 80 °C (red). **B** with respect to T^{45} position in the initial structure shows an inward-closed orientation of T^{45} at 40, 50 and 80 °C, while outward-open orientation at 60 °C. **C** The distance between two catalytic T^{45} and T^{125} in the modeling structure with respect to T^{20} and T^{100} from the template structure 4PGA (magenta). Larger distance with respect to 4PGA indicates an open catalytic loop, while less than or close to equal indicates a close state

increased susceptibility to substrate types. On the other hand, considering the ASFL (red ASFL; Fig. 5A), which certainly appears distorted, in comparison to the structure at 60℃. Concluding, 60℃ is the most optimal temperature for Asn_PA's catalytic activity.

Enzyme structure becomes stable and compact at elevated temperature as shown by Rg and *SASA* data

The gyration plot analysis over the MD run of 30 ns depicted relatable results as were obtained from RMSD calculations. The Rg plots showed the compactness of the solute within the system. A comparative Rg plot for each system with varied temperatures (Fig. 6A), where the black, red, and green lines depict 40, 50, 60, and, 80 °C, respectively. The observed degree of compactness lay between 2.5 to 3 nm. The protein in a system of 40 °C temperature continuously showed variation in the degree of compactness throughout the MD run, while the protein at a temperature of 50 °C showed varied compactness up to 20 ns runs but later after 20 ns the protein compactness was stabilized. Whereas, in the case of desirable temperature i.e., 60 °C, the compactness of protein was initially high, and after a run of 10 ns the overall protein tends to obtain a dynamic conformational compactness throughout the run of 30 ns. Through the comparative compactness analysis of the systems, we can conclude that the experimental and computational studies correlate well with each other and thus confirm that the Asn_PA enzyme from *P. aeruginosa* CSPS4 is maximally stable at a temperature of 60℃ and probably showed maximum activity at this temperature which also correlates well with the RMSF calculation.

Besides, the solvent-accessible surface area of the protein also shows how compactly a biomolecule is packed within the solvent around it. The overall SASA value falls between 165 and 210nm^2. The SASA results also complimented the above computational analysis. It was observed that the SASA values for the Asn_PA enzyme were maximum at 40 °C (black) which indicates it to be more polar and accessible to the solvent (Fig. 5B). Whereas, the SASA value showed a gradual downfall with increasing temperature. The system at 60 °C showed a continuous decrease in SASA value up to 10 ns, while after 10 ns, the average SASA value was 174.92nm^2 indicating adequate polar and non-polar characteristics of the protein, thus, making it catalytically more available (Darnal et al. 2023), and the group reported optimum activity of l-asparaginase at 60 °C, which supports the results from this study. In agreement with the results of Rg, the protein at an even higher temperature showed enhanced compactness (blue), i.e., after 7 ns the protein does not show much folding and unfolding, indicating the stability of the protein at 80 °C. Whereas, the SASA values contradict the results by increasing the solubility of the protein by several folds after 5 ns, indicating exposure of polar residues. Besides, it also indicates that the protein adopts an

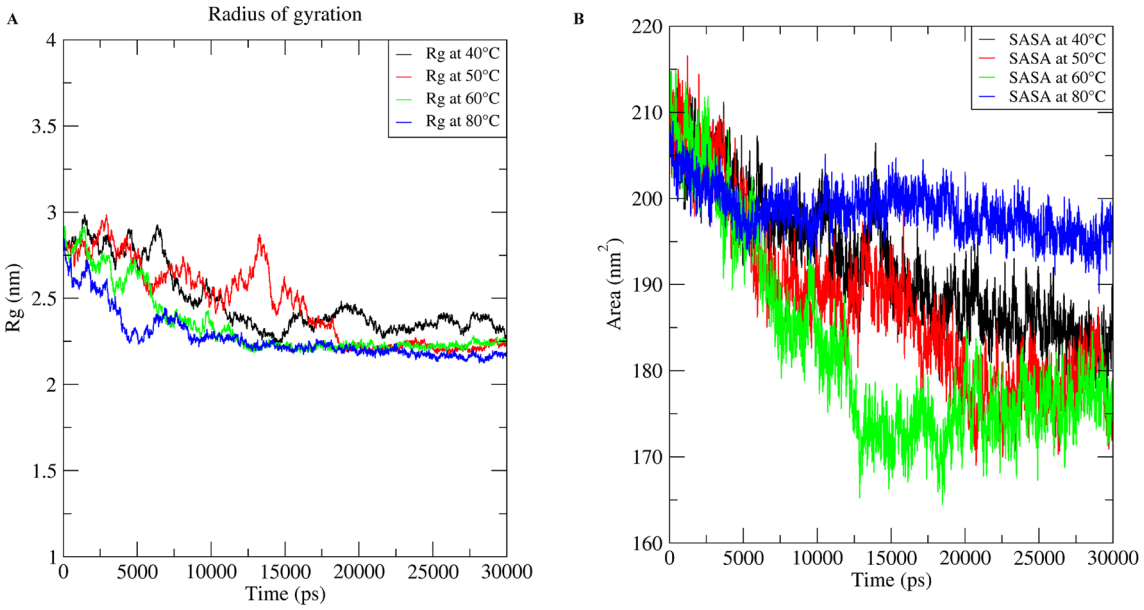

Fig. 6 The Rg also showed the compactness of the Asn_PA protein at different temperatures in a similar way as RMSD plots (**A**). The protein at 60 °C (green) showed the most stable and compact structure (**B**). The solvent-accessible surface area plot also showed the compactness of the protein based on the polarity of the residues toward the solvent

enhanced solubility after crossing the threshold temperature. Thus, we can clearly say that at 80 °C Asn_PA loses its catalytic activity even after enhanced stability. The catalytic domains adopt a non-specific conformation which leads to ineffective activity of Asn_PA at temperatures above 60 °C. Also, through the trajectory analysis for SASA parameters, which signifies its compactness over the time duration and makes it dynamically functional at 60 °C (Fig. 6B). In conclusion, protein stability increases with temperature rise but for Asn_PA, the catalytically most active state is acquired at 60 °C for several L-asparaginase of various sources (El-Naggar et al. 2016; Qeshmi et al. 2018).

Discussion

In recent years, a handful of asparaginases of *Pseudomonas* spp. have also been explored for their applicability in pharmaceutical and starch-based food industries (Saeed et al. 2018; Fatima et al. 2019; Kornbrust et al. 2009; Meghavarnam et al. 2018; Paul et al. 2020). However, little is known about the structural insights of asparaginases of *Pseudomonas* spp. To date, the PDB database consists of crystal structures of asparaginases from three different *Pseudomonas* spp. only which includes *P. putida* KT2440, *Pseudomonas* sp.7A, and, *P. aeruginosa* PA01. Therefore, the PDB database needs to be enriched by generating more crystal structures. Computational-based methods provide an extensive analysis of the desired protein by speedily exploring its sequence and structural information (Dadwal et al. 2023). The thermophilic characteristics of the Asn_PA enzyme (Kumar et al. 2024) of the present investigation encouraged to exploration of its structural insights using in silico analysis. An amplicon from *P. aeruginosa* CSPS4 showed 100% identity with the asparaginase encoding gene (*asnB*) of *P. aeruginosa* POA1 of 1089 bp. Most of the asparaginases from *Pseudomonas* spp. exhibit gene size near 1 kb corresponds to approximately 35 kDa protein and thus corroborates the findings of this investigation (El-Sharkawy et al. 2016; Saeed et al. 2018; Kumar et al. 2022; Qeshmi et al. 2022). Physiological characteristics showed that the current asparaginase is neutral type due to its theoretical pI of 7.07. Previous investigations report an alkaline optimum pH among most of the asparaginases of *Pseudomonas* type (El-Sharkawy et al. 2016; Qeshmi et al. 2022; Kumar et al. 2022). As a result, the Asn_PA was isolated and examined for its biophysical and biochemical characteristics, which revealed Asn_PA as a thermostable enzyme (Kumar et al. 2024).

Furthermore, the instability (li) and aliphatic index (Ai) of the Asn_PA were 29.80 and 95.72 respectively indicating that the protein is stable at higher temperatures. The Ai of MtBgl3c was 78.24 which was characterized as thermostable β-glucosidase (Dadwal et al. 2023). The GRAVY index of asparaginase of this investigation falls in the negative region and thus categorizes it as a hydrophilic protein (Gasteiger et al. 2005). Sequence analysis identified three conserved signature sequences like other asparaginases of bacterial

type (Kumar et al. 2022; Qeshmi et al. 2022). Besides, two catalytically important residues (T^{45} and T^{125}) were observed in two different putative conserved regions (LIVM]-x-{L}-T-G(2)-T-[IV]-[AGS] and ([GA]-x-[LIVM]-x(2)-H-G-T-D-T-[LIVM]) like other asparaginases (Bonthron and Jaskólski 1997; Hofmann et al. 1999; Qeshmi et al. 2022). Where, T-G-G-T and H-G-T-D-T amino acids were fully conserved in motif 1 and motif 2 respectively and it was like HR03Asnase of *P. aeruginosa* HR03 strain (Qeshmi et al. 2022).

Despite reliable approaches to x-ray crystallography and NMR, computational-based three-dimensional homology modeling is one of the preferred approaches to rationally predict a reliable model of a protein (Xiang 2006). Here, four methods (Phyre2, *i*-Tasser, Alpha Fold, and, MODELLER) were attempted to predict the most accurate model. MODELLER software provided the best 3D model based on residues in the favoured regions, the least residues in the disallowed region, and the DOPE score (−38,579.18; model no. 3) (Supplementary Table 1). MODELLER is a freely accessible software for predicting the 3D model of a protein using homology modelling (Webb and Sali 2016).

The Asn_PA structure generally consists of alpha helices, strands, and, coils, which make the structure flexible and mobile in nature, allowing various conformational adaptations for different substrates, ligands, water, and, metal ions (Liao et al. 2019; Kamalesh et al. 2020). It comprises mainly two domains, where the N-terminal domain exhibited most conserved residues, similar structure of asparaginases has been reported from *P. aeruginosa* and *P. putida* KT2440 (6WZ8) [Saeed et al. 2018; Strzelczyk et al. 2020; Qeshmi et al. 2022; Kumar et al. 2022]. The model generated through homology modeling was well superimposed against the template 4PGA, with an RMSD of 0.23Å. In 4PGA structure, the active site loop is reported in a closed conformation in the presence of ammonium ions as reported for the loop region between Thr^{20}-Gly^{40} as active site loop (Jakob et al. 1997). Besides, the active site residues were identified in the conserved motifs that were adjacent to each other which suggests that the protein behaves like another asparaginase superfamily. Moreover, RAMPAGE analysis showed that 94% of residues were in the favoured region and merely 0.3% of residues were in the disallowed region which shows confidence for the predicted model (Lovell et al. 2003). The ERRAT score of 91.46% further validates the model which predicts the statistics of non-bonded atom-to-atom interactions in a model (Colovos and Yeates 1993) **(Fig. S3).**

Docking studies unveiled that the Asn_PA exhibits catalytic activity towards asparagine and glutamine and thus classified as an asparaginase-glutaminase type enzyme. Asparaginase of *Pseudomonas* 7A having maximum structural similarity with Asn_PA also showed glutaminase activity (Jakob et al. 1997). Similar dual-activity was reported from asparaginases of *Pseudomonas* sp. PCH44 (Kumar et al. 2022), as well as other genera (Wade et al. 1971; Mahajan et al. 2012; Duval et al. 2002; Lopes et al. 2017). Though, glutaminase-free asparaginases have also been reported from a few species of *Pseudomonas* (Husain et al. 2016; Kumar et al. 2019).

Later, in this study molecular dynamics approach was employed to investigate the effect of temperature change on Asn_PA. While numerous studies have focused on optimizing the pH range, substrate source and, temperature to enhance asparaginase production (Rahimzadeh et al. 2016; Abhini et al. 2022; Darnal et al. 2023), however, limited information is available on a molecular-level understanding of asparaginases. MD analysis showed the functional activity of asparaginase at 60 °C as reported in previous investigations (El-Naggar et al. 2016). The N-terminal domain comprises FGE, which is not well studied in bacteria and, in the absence of substrate they remain disordered (Loch et al. 2021). The FGE forms the flexible active site loop, comprising Thr^{20}-Gly^{40} residues for 4PGA in a closed conformation, which in the case of Asn_PA falls between Thr^{45}-Pro^{65} residues based on structural superimposition and alignment. The initial structure generated for the Asn_PA was in a closed conformation with respect to 4PGA (Jakob et al. 1997). Later, with respect to a small temperature range molecular events were observed for the protein through MD analysis. The temperature ranges were set based on required threshold values with respect to experimental data (Kumar et al. 2024). The presence or absence of the substrates (asparagine or glutamine), alters the conformation of the active site loop or the FGE might remain lightly packed i.e., remain in a closed conformation in the presence of substrates (Kamalesh et al. 2022). Whereas, through the trajectory analysis of the Asn_PA in the absence of the substrate, the FGE remained in an open conformation (Fig. 5A) and by measuring the distance of T^{45} with respect to the initial structure (closed conformation). The measured distance for T^{45} at 60 °C is 3.3 Å in an outward open orientation, whereas in case of 40, 50 and, 80 °C, T^{45} showed inward closed orientation with a distance of 3.8, 1.6 and, 1.6 Å respectively (Loch et al. 2021). T^{45} was identified as a catalytic site of ASP_PA, and outward open conformation is probably contributed by thermal stability (Liao et al. 2019). On the contrary, protein at 80℃ overlaps with the closed conformation states in this case. The template of 4PGA is crystalized in a closed conformation in the presence of sulfur ions as an opportunistic substrate, where the distance between the two catalytically important T^{20} and T^{100} are at a distance of 7.2 Å. For Asn_PA, the distance between respective threonine T^{45} and T^{125} at 30, 40 and 50 °C is 7.3, 6.5 and 7.7 Å respectively (Fig. 5C). The increased distance (7.7 Å) between T^{45} and T^{125} at 60℃ supports open conformation of the enzyme, whereas 7.3 Å and 6.5 Å in correspond with 4PGA distance

(7.2 Å) show closed active site loop conformation at 40 °C and 50 °C respectively. Additionally, at 50 °C the distance reduced even further, indicating a closed-inactive loop, making the site unavailable for substrate at this temperature. Thus, it may be hypothesized that the Asn_PA showed maximum expansion and open state conformation at 60℃ in the absence of substrate due to the enhanced effect of temperature, i.e., the active site loop remains in an open state orientation at higher temperatures. Also, shown at 80℃, the distance up to 8.4 Å indicates an even wider cavity, either indicating substrate selectivity or active pocket distortion. Besides, the T^{45} outward open conformation at 60℃ supports the same, while for both the other two cases T45 does not support open conformation with respect to the initial structure (Fig. 5B and C). Whereas, in the absence of the substrate, the protein at temperatures 40 and 50℃ appeared compact or in a partially closed orientation even in the absence of substrates, which contradicts the activity of the enzyme due to the behavior of the flexible active loop as reported (Kamalesh et al. 2022). With respect to T^{45} in the initial structure, at 40 and 50 °C uptake an inward close conformation with a distance of 3.8 Å and 1.6 Å, while at 60 °C T^{45} uptakes an outward open conformation with a distance of 3.3 Å from initial structure, again supporting enzyme as active at 60 °C. Thereafter, it suggests that the present asparaginase may exhibit a closed orientation in the presence of the substrate and show maximum catalytic activity in comparison to the lower temperatures of 40 and 50 °C where they remain in an inactive orientation. Through the trajectory analysis, it was observed that RMSD, Rg, and, SASA values correlate well with each other in each temperature case and all performed analyses. Even the RMSF analysis also reciprocated the same results concerning residues of interest. From the RMSD analysis, it was observed that the Asn_PA enzyme at 60 °C quickly converges within 10 ns, despite being in a higher temperature range as compared to the other two cases (40 and 50 °C). This is the first such investigation on asparaginase of *Pseudomonas*. Likewise, Rg which shows the compactness of the protein also signified 60℃ as the most suitable temperature for the protein Asn_PA to remain in the catalytically inactive state in the absence of substrate. The ASFL region comprises eight alanines, replacing them specifically with another residue type can impact the stability of the enzyme at higher temperatures. Since, the alanine density in the active region is high so alternativity, substituting it with bulkier residue, charged or hydrophilic residues can alter different forms of interactions within the region (Fig. S4). Ala substitution by Ser and Thr has been reported in *T. thermophilus* HB27 to enhance protein structure stability (Kumwenda et al. 2013). For Asn-PA substitution of Ala with Ser, Thr, or Glu and Lys can be a futuristic topic of separate experiments. The SASA analysis also assessed that 60℃ is the most suitable temperature for the current protein for enzymatic activity. At this temperature, the Asn_PA remained oriented in a confined order without making the core or catalytic domain exposed to the solvent. In conclusion, the higher temperature directly relates to more mobility of the molecules and the deformations but since the targeted protein is temperature tolerant, thus, shows significant results at its favorable temperature. Foremost, the protein folding and dynamics not just only depend on the amino acid composition but also on factors like water, temperature, solvent, pH, electrical charges, and, other factors. However, in this work, the considered factors are protein, solvent, and, temperature, which directly influence the strength of hydrophobic and hydrophilic interactions and thus, the folding and unfolding occur with the change of solvent temperatures immediately. Furthermore, the active site is present as flexible loop, which embarks the flexibility of the asparaginase enzyme to adapt to physiological changes, and to the substrate's specificity (Nguyen et al. 2017). Thus, the Asn_PA exhibits most favorable and enhanced catalytic activity at 60℃, which proposes it as an adequate therapeutic source for industrial purposes.

Conclusion

Sequence analysis of the Asn_PA protein showed that it exhibits theoretical pI at neutral pH and a putative molecular weight of 39.82 kDa. Further, it showed three highly conserved motifs, of them, two motifs consisting of catalytically critical threonine residues. Homology modeling of Asn_PA and further structural analysis showed a flexible folded structure present towards the N-terminal domain, which might undergo conformational changes on elevation of temperature and regulate the catalytic activity of the enzyme. Docking studies showed its possible catalytic activity on the asparagine as well as glutamine substrates, which classify it as an asparaginase-glutaminase type asparaginase enzyme. MD analysis unveiled that the Asn_PA exhibits better catalytic activity at 60 °C, distinguishing this enzyme from the other available asparaginases from *Pseudomonas* spp. The RMSD, Rg, and, SASA profiles were well correlated at varying temperatures to support the catalytic behavior of the Asn_PA protein with each other in each temperature case. The ASFL stretches revealed that in the Asn-PA, substituting alanine with serine, threonine, glutamine, or lysine can be a futuristic approach to enhance the thermostability of the protein. This is the first such report on thermophilic asparaginase from mesophilic *P. aeruginosa* strain which finds applicability in starch-based food industries.

Supplementary Information The online version contains supplementary material available at https://doi.org/10.1007/s13205-024-04072-w.

Acknowledgements Authors are thankful to Babasaheb Bhimrao Ambedkar University (BBAU), Lucknow, India, and Gautam Buddha Central Library, BBAU, Lucknow, India for providing infrastructure and access to several journals and other useful online resources.

Author contributions DV and YA conceived the idea. VK and PA performed the experimental analysis. AS helped in data analysis. DV, VK, PA, and YA wrote the manuscript. DV has coordinated the complete study. All the authors read and approved the final version of the manuscript.

Funding DV and YA are grateful to the Council of Science and Technology, Uttar Pradesh, India for providing financial assistance (CST-D/1552). The authors have no relevant financial or non-financial interests to disclose.

Data availability The gene sequence of *Asn_PA* is submitted to GenBank with accession no. OR509736.

Declarations

Conflict of interest The authors declare no conflict of interest.

Research involving human participants and/or animals Not applicable.

Consent for publication On acceptance of the manuscript the copyright from the author will be transferred to the journal.

Informed consent Not applicable.

References

Abhini KN, Rajan AB, Zuhara KF, Sebastian D (2022) Response surface methodological optimization of l-asparaginase production from the medicinal plant endophyte *Acinetobacter baumannii* ZAS1. J Gent EnggBiotechnol 20:22

Arjun JK, Aneesh B, Kavitha T, Krishnan KH (2016) Therapeutic L-Asparaginase activity of bacteria isolated from marine sediments. Int J Pharm Sci Drug Res 8(4):229–234

Batool T, Makky EA, Jalal M, Yusoff MM (2016) A comprehensive review on L-Asparaginase and its applications. Appl Biochem Biotechnol 178(5):900–923. https://doi.org/10.1007/s12010-015-1917-3

Bhardwaj A, Leelavathi S, Mazumdar-Leighton S, Ghosh A, Ramakumar S, Reddy VS (2010) The critical role of N-and C-terminal contact in protein stability and folding of a family 10 xylanase under extreme conditions. PLoS One 5:11347

Bonthron DT, Jaskolski M (1997) Why a "benign" mutation kills enzyme activity. Structure-based analysis of the A176V mutant of *Saccharomyces cerevisiae* L-Assparaginase I. Acta Biochim Pol 44:491–504

Broome JD (1961) Evidence that the L-Asparaginase activity of guinea pig serum is responsible for its anti-lymphoma effects. Nature 191:1114–1115

Burke MJ, Rheingold SR (2017) Differentiating hypersensitivity versus infusion-related reactions in paediatric patients receiving intravenous asparaginase therapy for acute lymphoblastic leukemia. Leuk Lymphoma 58:540–551

Cachumba JJ, Antunes FA, Peres GF, Brumano LP, Santos JC, Da Silva SS (2016) Current applications and different approaches for microbial l-Asparaginase production. Brazilian J Microbiol 47:77–85

Colovos C, Yeates TO (1993) Verification of protein structures: patterns of nonbonded atomic interactions. Protein Sci 2:1511–1519

Dadwal A, Sharma S, Satyanarayana T (2023) Biochemical characteristics of *Myceliophthorathermophila* recombinant β-glucosidase (MtBgl3c) applicable in cellulose bioconversion. Prep Biochem Biotechnol 17:1–12

Darnal S, Patial V, Kumar V, Kumar S, Kumar V, Padwad YS, Singh D (2023) Biochemical characterization of extremozyme L-Asparaginase from *Pseudomonas* sp. PCH199 for therapeutics. AMB Express 13:22

DeSantis F, Miotto M, Di Rienzo L, Milanetti E, Ruocco G (2022) Spatial organization of hydrophobic and charged residues affects protein thermal stability and binding affinity. Scient Rep 12:12087. https://doi.org/10.1038/s41598-022-16338-5

Duval M, Suciu S, Ferster A, Rialland X, Nelken B, Lutz P, Philippe N (2002) Comparison of *Escherichia coli*–asparaginase with *Erwinia*-asparaginase in the treatment of childhood lymphoid malignancies: results of a randomized European Organisation for Research and Treatment of Cancer—Children's Leukemia Group phase 3 trial. Blood J Am Soc Hematol 99:2734–2739

El-Naggar NA, Deraz S, Soliman H (2016) Purification, characterization, cytotoxicity, and anticancer activities of L-asparaginase, anti-colon cancer protein, from the newly isolated alkaliphilic Streptomyces fradiae NEAE-82. Sci Rep 6:32926

El-Sharkawy AS, Farag AM, Embaby AM, Saeed H, El-Shenawy M (2016) Cloning, expression, and characterization of aeruginosa EGYII L-Asparaginase from Pseudomonas aeruginosa strain EGYII DSM 101801 in E. coli BL21 (DE3) pLysS. J Mol Catal B Enzym 132:16–23

Farag AM, Hassan SW, Beltagy EA, El-Shenawy MA (2015) Optimization of production of anti-tumor L-Asparaginase by free and immobilized marine *Aspergillus terreus*. The Egyptian J Aquat Res 41:295–302

Fatima N, Khan MM, Khan IA (2019) L-asparaginase produced from soil isolates of *Pseudomonas aeruginosa* shows potent anti-cancer activity on HeLa cells. Saudi J Biol Sci 6:1146–1153

Gasteiger E, Hoogland C, Gattiker A, Duvaud SE, Wilkins MR, Appel RD, Bairoch A (2005) Protein identification and analysis tools on the ExPASy server Humana press 571–607

Guruprasad K, Reddy BB, Pandit MW (1990) Correlation between stability of a protein and its dipeptide composition: a novel approach for predicting in vivo stability of a protein from its primary sequence. Protein Eng Des Sel 4:155–161

Hijiya N, Van Der Sluis IM (2023) Asparaginase-associated toxicity in children with acute lymphoblastic leukaemia. Leuk Lymphoma 57:748–757

Hofmann K, Bucher P, Falquet L, Bairoch A (1999) The PROSITE database, its status in 1999. Nucleic Acids Res 27(1):215–9

Husain I, Sharma A, Kumar S, Malik F (2016) Purification and characterization of glutaminase free asparaginase from *Pseudomonas otitidis*: induce apoptosis in human leukemia MOLT-4 cells. Biochimie 121:38–51

Ikai A (1980) Thermostability and aliphatic index of globular proteins. The J Biochem 88:1895–1898

Jakob CG, Lewinski K, Lacount MW, Roberts J, Lebioda L (1997) Ion binding induces closed conformation in Pseudomonas 7A glutaminase-asparaginase (PGA): Crystal structure of the PGA-SO42–NH4+ complex at 1.7Å resolution. Biochem 36:923–931

Ji W, Yuan C, Chakraborty P, Gilead S, Yan X, Gazit E (2019) Stoichiometry-controlled secondary structure transition of amyloid-derived supramolecular dipeptide co-assemblies. Commun Chem 2(1):65

Juluri KR, Siu C, Cassaday RD (2022) Asparaginase in the treatment of acute lymphoblastic leukemia in adults: current evidence and place in therapy. Blood Lymphat Cancer 12:55–79

Kamalesh D, Nair A, Sreeshma J, Arundhathi PS, Sudandiradoss C (2020) Statistical and molecular dynamics (MD) simulation approach to investigate the role of intrinsically disordered regions of shikimate dehydrogenase in microorganisms surviving at different temperatures. Extremophiles 24:831–842

Kamalesh A, Loch JI, Karlowski WM, Jaskolski M (2022) Massive annotation of bacterial L-Asparaginases reveals their puzzling distribution and frequent gene transfer events. Sci Rep 12:15797

Kelley LA, Mezulis S, Yates CM, Wass MN, Sternberg MJ (2015) The Phyre2 web portal for protein modeling, prediction, and analysis. Nature Prot 10:845–858

Knott SR, Wagenblast E, Khan S, Kim SY, Soto M (2018) Asparagine bioavailability governs metastasis in a model of breast cancer. Nature 554:378–381

Kornbrust BA, Stringer MA, Lange NEK, Hendriksen HV, Whitehurst R, Oort M (2009) Asparaginase an enzyme for acrylamide reduction in food products. Enz Food Technol 2:59–87

Kumar V, Kumar S, Darnal S, Patial V, Singh A, Thakur V, Singh D (2019) Optimized chromogenic dyes-based identification and quantitative evaluation of bacterial L-Asparaginase with low/no glutaminase activity bio-prospected from pristine niches in Indian trans-Himalaya. 3 Biotech 9:1–9

Kumar S, Darnal S, Patial V, Kumar V, Kumar V, Kumar S, Singh D (2022) Molecular cloning, characterization, and in silico analysis of L-Asparaginase from Himalayan Pseudomonas sp. PCH44. 3 Biotech 8:162

Kumar V, Kumar SV, Kumar R, Sharma S, Shah A, Chaturvedi CP, Verma D (2024) Cloning, expression, and characterization of a novel thermo-acidophilic L-Asparaginase of Pseudomonas aeruginosa CSPS4. 3 Biotech. https://doi.org/10.1007/s13205-024-03916-9

Kumwenda B, Litthauer D, Bishop OT, Reva O (2013) Analysis of protein thermostability enhancing factors in industrially important *Thermus* bacteria species. Evol Bioinform Online 9:327–342. https://doi.org/10.4137/EBO.S12539

Kyte J, Doolittle RF (1982) A simple method for displaying the hydropathic character of a protein. J Mol Biol 157:105–132

Laskowski RA, Swindells MB (2011) LigPlot+: multiple ligand-protein interaction diagrams for drug discovery. J Chem Inf Model 51:2778–2786

Liao ML, Somero GN, Dong YW (2019) Comparing mutagenesis and simulations as tools for identifying functionally important sequence changes for protein thermal adaptation. Proc Natl Acad Sci 116:679–688

Lindahl E, Hess B, Van Der Spoel D (2001) GROMACS 3.0: a package for molecular simulation and trajectory analysis. Mol Model Annual 7:306–317

Loch JI, Jaskolski M (2021) Structural and biophysical aspects of l-asparaginase: a growing family with amazing diversity. IUCR J 8:514–531

Lopes AM, Oliveira-Nascimento LD, Ribeiro A, Tairum CA Jr, Breyer CA (2017) Therapeutic L-Asparaginase: upstream, downstream, and beyond. Critic Rev Biotechnol 37:82–99

Lovell SC, Davis IW, Arendall WB III, De Bakker PI et al (2003) Structure validation by Cα geometry: ϕ, ψ, and Cβ deviation. Proteins 50:437–450

Lubkowski J, Vanegas J, Chan WK, Lorenzi PL, Weinstein JN, Wlodawer A (2020) Mechanism of catalysis by l-asparaginase. Biochemistry 59:1927–1945

Mahajan RV, Saran S, Kameswaran K, Saxena RK (2012) Efficient production of l-asparaginase from *Bacillus licheniformis* with low-glutaminase activity: optimization, scale up and acrylamide degradation studies. Bioresource Technolol 125:11–16

Marti D, Torras J, Bertran O, Turon P, Aleman C (2021) Temperature effect on the SARS-CoV-2: amolecular dynamic study of the spike homotrimeric glycoprotein. Comput Struct Biotechnol J 19:1848–1862

Meghavarnam AK, Janakiraman S (2018) Evaluation of acrylamide reduction potential of l-asparaginase from *Fusarium culmorum* (ASP-87) in starchy products. LWT 89:32–37

Merck (2000) Elspar Asparaginase. Deerfield, IL: Ovation Pharmaceuticals

Mottram DS, Wedzicha BL, Dodson AT (2002) Acrylamide is formed in the Maillard reaction. Nature 419:448–449

Nagarethinam S, Naik AN, Udupa N, Rao VJ, Vanathi MB (2012) Microbial l-asparaginase and its future prospects. Asian J Med Res 1:159–160

Nguyen HA, Durden DL, Lavie A (2017) The differential ability of asparagine and glutamine in promoting the closed/active enzyme conformation rationalizes the *Wolinella succinogenes* l-asparaginase substrate specificity. Sci Rep 7:1–41643

Oostenbrink C, Villa A, Mark AE, Van Gunsteren WF (2004) A biomolecular force field based on the free enthalpy of hydration and solvation: the GROMOS force-field parameter sets 53A5 and 53A6. J Comput Chem 25:1656–1676

Patel PG, Panseriya HZ, Vala AK, Dave BP, Gosai HB (2022) Exploring current scenario and developments in the field of microbial l-asparaginase production and applications: a review. Process Biochem 121:529–541

Paul V, Tiwary BN (2020) An investigation on the acrylamide mitigation potential of l-asparaginase from *Aspergillus terreus* BV-C strain. Biocat Agri Biotechnol 27:101677

Pol-Fachin L, Rusu VH, Verli H, Lins RD (2012) GROMOS 53A6GLYC, an improved GROMOS force field for hexopyranose-based carbohydrates. J Chem Theory Comput 11:4681–4690

Qeshmi FI, Homaei A, Fernandes P, Javadpour S (2018) Marine microbial L-asparaginase: biochemistry, molecular approaches, and applications in tumor therapy and in food industry. Microbiol Res 208:99–112

Qeshmi FI, Homaei A, Khajeh K, Kamrani E, Fernandes P (2022) Production of a novel marine *Pseudomonas aeruginosa* recombinant L-Asparaginase: Insight on the structure and biochemical characterization. Marine Biotechnol 24:599–613

Rahimzadeh M, Poodat M, Javadpour S, Qeshmi FI, Shamsipour F (2016) Purification, characterization, and comparison between two new l-asparaginases from *Bacillus* PG03 and *Bacillus* PG04. The Open Biochemi J 10:35

Ren Y, Soy S, Ding Y, Iqbal J, Broome JD (2004) Methylation of the asparagine synthetase promoter in human leukemic cell lines is associated with a specific methyl binding protein. Oncogene 23:3953–3961

Saeed H, Soudan H, El Sharkawy A, Farag A, Embaby A, Ataya F (2018) Expression and functional characterization of *Pseudomonas aeruginosa* recombinant L-Asparaginase. The Protein J 37:461–471

Shamsir MS, Dalby AR (2007) β-Sheet containment by flanking prolines: Molecular dynamic simulations of the inhibition of β-sheet elongation by proline residues in human prion protein. Biophys J 92(6):2080–2089

Sigrist CJ, Cerutti L, Hulo N, Gattiker A, Falquet L (2002) PROSITE: a documented database using patterns and profiles as motif descriptors. Brief Bioinfo 3:265–274

Strzelczyk P, Zhang D, Dyba M, Wlodawer A, Lubkowski J (2020) Generalized enzymatic mechanism of catalysis by tetrameric l-asparaginases from mesophilic bacteria. Sci Rep 10:17516

Tareke E, Rydberg P, Karlsson P, Eriksson S, Tornqvist M (2002) Analysis of acrylamide, a carcinogen formed in heated foodstuffs. J Agricul Food Chem 50:4998–5006

Tosta Perez M, Herrera Belén L, Letelier P, Calle Y, Pessoa A, Farías JG (2023) L-Asparaginase as the gold standard in the treatment

of acute lymphoblastic leukemia: a comprehensive review. Med Oncol 40:5–150
Van Trimpont M, Peeters E, De Visser Y, Schalk AM, Mondelaers V, De Moerloose B, Lavie A, Lammens T, Goossens S, Van Vlierberghe P (2022) Novel insights on the use of L-Asparaginase as an efficient and safe anti-cancer therapy. Cancers 14:4–902. https://doi.org/10.3390/cancers14040902
Wade HE, Robinson HK, Phillips BW (1971) Asparaginase and glutaminase activities of bacteria. Microbiol 69:299–312
Webb B, Sali A (2016) Comparative protein structure modeling using MODELLER. Curr Prot Bioinfo 54:561–5637
Worton KS, Kerbel RS, Andrulis IL (1991) Hypomethylation and reactivation of the asparagine synthetase gene induced by L-Asparaginase and ethyl methane-sulfonate. Cancer Res 51:985–989
Xiang Z (2006) Advances in homology protein structure modeling. Curr Prot Peptide Sci 7:217–227
Xu F, Oruna-Concha MJ, Elmore JS (2016) The use of asparaginase to reduce acrylamide levels in cooked food. Food Chem 210:163–171. https://doi.org/10.1016/j.foodchem.2016.04.105
Yuan S, Chan HS, Hu Z (2017) Using PyMOL as a platform for computational drug design. Wiley Interdisciplin Rev Comput Mol Sci 7:e1298
Zhou X, Zheng W, Li Y, Pearce R, Zhang C, Bell E, Zhang G, Zhang Y (2022) i-TASSER-MTD: a deep-learning based platform for multi-domain protein structure and function prediction. Nat Prot 10:2326–2353